

TIM: Tree Imaging Machine for low-cost digital images of tree cores and cookies

Your Name

April 2, 2025

Abstract

Studies of tree rings from climatology to ecology have benefitted recently from new methods to image wood rapidly and efficiently, helping to scale up the number and quality of image samples. Current approaches are, however, limited in scanning dimensionality and can be cost-prohibitive. The Tree Imaging Machine (TIM) is a do-it-yourself scanning tool made to digitize tree cookies and cores that address these limitations. TIM takes partially overlapping microscopic images of samples and stitches the individual images together to form a mosaic, which can be zoomed in to visualize features on the scale of 0.01 mm. With scans of up to 21 140 DPI, TIM produces one of the highest resolution images among similar tools for the competitive price of less than \$3 000 USD. We designed TIM to have a large working plane to allow digitizing cores over 50 cm and complete cookies. Operators can prepare sample batches of multiple cores and cookies, letting the machine work until the queue is finished. All of the 3D printed parts are available for download on the [NIH 3D printing repository](<https://doi.org/10.60705/3DPX/21561.3>) and the software is open source, with instructions to recreate this tool available on [GitHub](<https://github.com/temporalecologylab/TreeRings>). TIM provides an important advance in scanning resolution, tree cookie sampling, maximum core sample size, batch digitization, and cost in a single package. This promotes the digitization of larger samples and can collect data at finer resolutions in an open-source design which can be built on and improved as new technologies become available.

1 Introduction

Incremental growth rings from trees have provided valuable insights into the abiotic and biotic environment across multiple fields—from climatology to forestry and ecology. Dated tree rings from dendrochronology have been critical to reconstructing past climates of regional and local environments, providing the most accurate, precise, and reliable dating among alternatives (Mann *et al.*, 1999), and thus fundamentally informing our understanding of climate change today (Fritts, 1971; Williams *et al.*, 2010; Guijal & Guiot, 2021; Sheppard, 2010). They are also increasingly used in ecology to understand how plant competition affects tree growth in addition to climate (Buechling *et al.*, 2017) and have implications in forestry to managing stand dynamics (Canham *et al.*, 2004). These fields have leveraged two basic types of tree sampling techniques to capture the variation of tree rings: cores, which are cylindrical samples collected using an incremental

borer, and ‘cookies,’ which are entire cross sections (and thus allow measuring as many radii from the sample as desired, Speer, 2010). As understanding tree growth and managing forest becomes more critical to mitigating climate change, scaling up the collection and processing of tree ring samples has become increasingly important.

The first computer-based method to measure tree ring widths used a microcomputer, a stage micrometer, and a push button. With this technique, still used widely today, a trained technician shifts a core underneath a microscope objective and pushes a button connected to a microcomputer to record a ring’s location (Robinson & Evans, 1980). This method has high precision but depends heavily on specific technicians and maintains no image record (Levanič, 2007).

Image analysis of tree rings was later implemented to reduce both errors in sampling and sampling bias across individual technicians, with major methods developed in the 1980s and 1990s to digitize tree ring samples using optical scanning (McMillin, 1982) (Guay *et al.*, 1992). Optical scanners are still readily available for purchase, using a top of the line scanner, like the Epson Perfection V850 Pro produces maximum resolutions of 6 400 dpi and scan an area of up to 21.6 cm x 29.7 cm. More recent techniques have aimed to achieve higher resolutions and/or larger samples through a different digitization approach—using an image-capturing system. These systems rely on a microscope camera to take images, motors to move the sample or camera, a computer to manage the capturing, and a second, more powerful, computer to stitch images into a larger composite image. Decreasing the field of view of each captured image increases the resolution of the final stitched image without restricting the size of the sample (Muhlich *et al.*, 2022). Stitching multiple images into one mosaic is a common technique used in other fields such as mineralogy and cellular biology (Ro & Kim, 2021; Mohammadi *et al.*, 2024), which was first implemented for tree rings through the Advanced Tree-Ring Image Capturing System (ATRICS) (Levanič, 2007).

Since ATRICS was introduced in 2007, image capture and stitching of tree rings have become more common. Today CaptuRING offers a more modern do-it-yourself alternative to ATRICS, creating scans up to 5 339 dpi using a DSLR camera and motorized stage (García-Hidalgo *et al.*, 2022). Another alternative, Gigapixel, achieves an impressive 19 812 dpi with the same DSLR image capture and composite stitch method (Griffin *et al.*, 2021). While CaptuRING and Gigapixel both use DSLR cameras and motorized movement, they differ on two fronts. First, Gigapixel’s camera is traversed across a stationary sample while CaptuRING moves a core sample underneath a stationary camera. With a mobile camera, multiple samples can be recorded sequentially without needing to remove a sample from a stage upon image completion—significantly reducing the active setup time for an operator. Second, Gigapixel automatically stitches individual images together once imaging is complete. This removes the need to transfer images to a more powerful computer for stitching as is necessary with CaptuRING. Additionally, both of these systems are designed to capture images along a singular axis as the entire width of a core fits within a single image’s field of view. This assumption fundamentally restricts the digitization to be limited only to cores, as cookies have a two dimensional scanning surface.

We made TIM to combine the open-source and open-hardware philosophies of CaptuRING with the functionality of Gigapixel. We added support to digitize both cookies and cores, increased the maximum sample length, perform image stitching directly without the need for manual file transfer, and capture batches of samples sequentially—all while minimizing cost. Our design requires the use of 3D printed components and com-

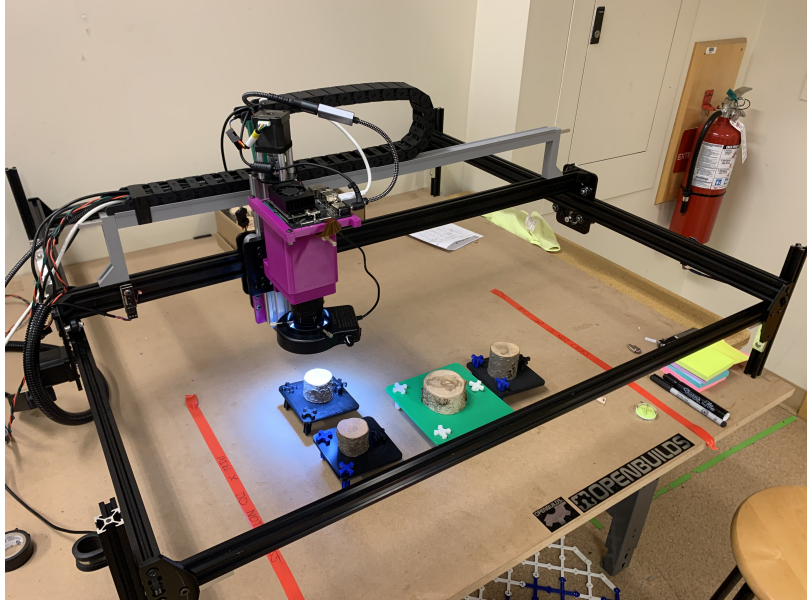


Figure 1: Complete assembly of TIM. Included in the work plane a few cookies ready to be scanned.

mon hand tools such as allen keys and wrenches. No specialized equipment or power tools are required beyond this. Excluding 3D printed parts, the total cost of the machine is approximately \$2 200 USD (compared to the \$70 000 USD of the Gigapixel, Griffin *et al.*, 2021). We chose to use a Raspberry Pi HQ camera with a microscope lens to save on purchasing a professional camera with a macro lens. Professional camera setups are comparable in price to the entire cost of TIM. Additional savings can also be had when factoring in the cost of a professional stitching software license such as PTGui, the suggested software to use with CaptuRING.

2 Methods

2.1 TIM System Design

TIM can be thought of as a combination of multiple subsystems: a gantry machine, camera, and computer (Figure 1). For the gantry machine, cartesian movement in the X , Y and Z directions is a result of two machine kits and a motor controller from OpenBuilds—the ACRO 1010, the NEMA 17 lead screw linear actuator, and the X32 Motor Controller running GRBL firmware. The machine kit includes extruded aluminum rails, carriages to slide along the rails, stepper motors to control the X and Y movement, and all the hardware to assemble the machine. To fit on the build plates of the ACRO system, we made an adapter to connect the linear actuator to the X and Y axis, thus creating motion in the Z axis. The size of the work plane is ultimately up to the size of the ACRO kit that is purchased—allowing for more flexibility. Building on top of kits allowed for quick assembly with sound instructions and saved development time. For the camera, we chose a 12MP Raspberry Pi HQ Camera equipped with a SEEED studio microscope lens and connected this to the gantry machine using custom adapters. For the computer, we implemented all of the software control, image stitching, and graphical user interface (GUI) to run on an NVIDIA Jetson Orin Nano (Jetson) which also connects to

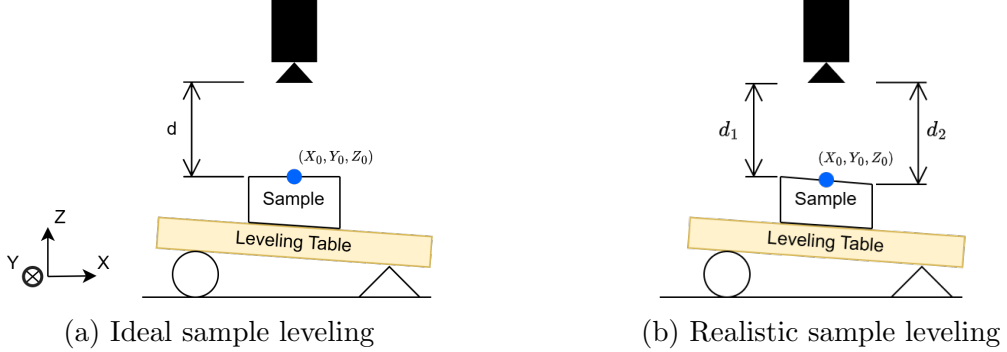


Figure 2: Side view of the camera and sample on top of a leveling table. The ideal sample leveling shows a uniform distance, d , at all XY coordinates on the sample. This is impossible to achieve in reality, the true sample leveling has a non uniform distance at unique XY .

the camera via a MIPI cable. Controlling the machine is done by launching a Python program and interacting with mouse button clicks on the GUI.

By choosing this combination, we were able to reduce the weight and cost of the camera significantly, which reduced design challenges in stabilizing movement of a heavier DSLR and allowed us to invest more in a powerful computer that can handle intensive image processing. The Jetson is an edge computer which drives a monitor for a GUI, sends commands to the motor controller to move the machine, runs image processing calculations for control, and performs calculations to stitch individual images into one mosaic. Despite the weight reductions, torsion on the gantry arm still resulted in a non-zero torsional deflection. A torsion correcting adapter was designed to counteract this rotation and level the lens.

2.2 Preparing Cookies and Cores

TIM can scan both tree cookies and tree cores. Sample preparation for both are equally important but require different approaches. The general guidelines used for preparing cookies and cores applies—requiring samples to be sanded with incrementally increasing sand paper grit to produce an even surface for scanning (Speer, 2010). We sanded cookies using an orbital sander with mesh sandpaper from 60 to 800 grit, then used a microscope to visually inspect the quality of the sanding. We considered the sample to be sufficiently prepared when vessels were easily identifiable.

TIM requires additional sanding considerations for each sample type. For cookies, it is important to have the top and bottom surfaces nearly parallel. Small differences in plane angle can be corrected using the 3D printed leveling table we designed (Figure 2a). For cores, care should be taken to maximize the scanning surface. This means removing material to be coincident to the center of the cross section of the core. Similarly to cookies, the scanning surface should be as close to parallel to the XY-plane as possible, but generally does not need to be leveled using the leveling tables. Cores also need to be aligned to be parallel to the Y axis to be digitized, using squaring tool or similar to help with alignment. Any warping in core mounts needs to be counteracted with the use of trigger clamps.

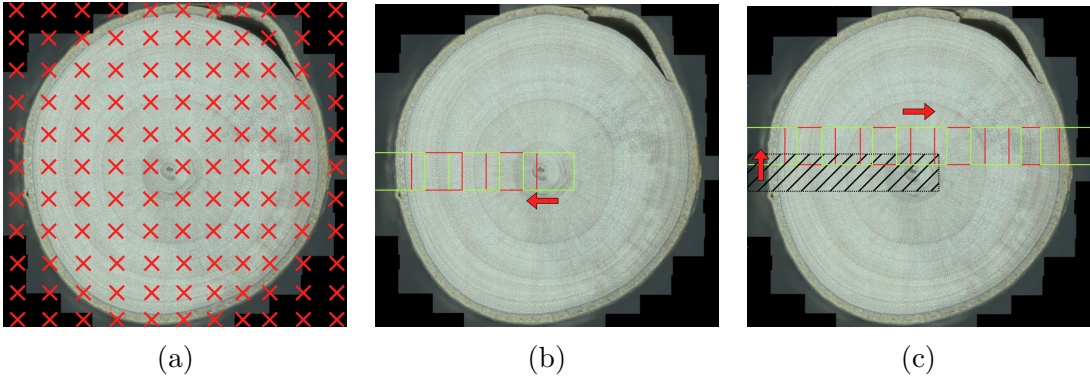


Figure 3: An example imaging process of a cookie sample. Here, the height and width are enclosed the entire surface area of the cookie and TIM begins by generating a grid of target coordinates to systematically capture a grid of continuous and partially overlapping images (a). TIM takes its first image at the center coordinate of the sample, then the rectangular field of view from the camera moves to adjacent target coordinates until it reaches the left boundary—capturing an image for each target coordinate (b). After completing the row, TIM moves to a new row and continues capturing adjacent images (c).

2.3 Sample Digitization

The subsystems of TIM can be best understood by following the process from sample setup through obtaining a stitched image. To achieve this with a fixed focus camera, the samples must be nearly orthogonal to the camera lens. Once the sample is level, the operator must follow a procedure to inform TIM of where the sample is, and the its size. To do this, the operator interacts with the machine using buttons on the GUI—navigating and focusing the camera on the center of the sample. The sample height and width in the X and Y dimensions are then entered in the GUI to be saved. Finally, the user must click the 'Add Sample' button which provides more fields to add sample identifiers and save the center coordinate. This procedure can be repeated to create a queue of samples to digitize as a batch. One additional parameter that needs to be defined is the height and width of the field of view of one image from the camera. We adjusted the focal length of the camera using the zoom ring to have a constant field of view of approximately 3 mm x 5 mm when in focus. The sample height and width, sample identifiers, sample type, sample center coordinate, and the height and width of an image provides sufficient information to digitize a sample.

2.3.1 Exhaustive Sample Traverse

The goal of this traversal is to obtain in-focus images that have a region of overlap with each of its neighbors—the basis of image stitching (Figure 3). Digitizing cores can be done without needing to traverse in both the X and Y axis. The optimal scanning path for a core is to align the length of cores to the Y axis and only take one column of images. Spanning the surface area of a cookie requires movement in both the X and Y axis.

2.3.2 Image Focusing

Centering the design of TIM around a fixed focus camera and lens meant we needed to focus the images with a software procedure. The only controllable parameter to focus a fixed focus lens is by changing the distance of the lens relative to the sample. With TIM's microscope lens, the depth of field of the image is sensitive enough that sub-millimeter heights can move an image out of focus. Solving this in a time-efficient manner involves two stages. We provide a complete glossary of notation used to describe the methods, see Table S1. The first stage takes advantage of the requirement to navigate and focus the camera to the center of the sample. This allows the initial Z_0 value, captured when adding a sample, to be an informed guess as to what value would have an in-focus image across the entire surface. From the first coordinate captured (X_0, Y_0, Z_0) , multiple images are taken at different heights (saved as a vector $\mathbf{Z}_{\text{samples}}$). The difference in height between each image are equally spaced, and are described by the relative distance to Z_0 in the vector $\boldsymbol{\delta}$. We found that it is important to have a distance of no more than 0.1 mm between each image in the stack to maximize the likelihood of an in-focus image at height Z_{focused} . With a sufficiently wide height range of 1 mm, TIM needs to take 11 images at different heights for comparison. The number of images taken is an editable parameter in the configuration file and can be increased, along with the height range, if in-focus images are not being obtained.

Our focusing procedure begins at 0.5 mm above Z_0 and finishes with the last image at 0.5 mm below Z_0 . The 11 images then have their normalized variance calculated in a separate thread to measure the image sharpness (Mir *et al.*, 2014). The image with the maximum score is saved and can be considered the most in-focus image, while the rest are deleted.

The second stage of our time-efficient focusing procedure uses a feedback loop to update the initial Z_0 at each image location (X_k, Y_k, Z_k) . Without a feedback loop, the sample alignment must have a difference in height no greater than 0.5 mm ($d_1 - d_2 < 0.5\text{mm}$ in Figure 2b). Rather than increasing this height range, a greater alignment error can be managed by adjusting the starting image height until Z_{focused} is at the center index of $\mathbf{Z}_{\text{samples}}$. The likelihood of an adjacent target (X_{k+1}, Y_{k+1}) containing an in-focus image is highest in this scenario. A negative feedback PID control algorithm is used to adjust the initial height of each image, with α_k , as the camera navigates the sample (O'Dwyer, 2000). This alleviates the need of having remarkably level sample alignment ($d_1 - d_2 < 0.5\text{mm}$ in Figure 2b).

$$\boldsymbol{\delta} = \begin{bmatrix} 0.5 \\ 0.4 \\ \vdots \\ -0.4 \\ -0.5 \end{bmatrix}$$

$$Z_{\text{focused}} \in \mathbf{Z}_{\text{samples}} = Z_0 + \boldsymbol{\delta} + \alpha_k$$

To reduce motion blur in the images, the range of $\mathbf{Z}_{\text{samples}}$ is traversed at constant velocity and images are captured without stopping. Decoupling the auxiliary camera control from the G-code commands to control the machine has shown to decrease digitization time and decrease vibrational effects from acceleration and deceleration (Propst & Mueller, 2025). This is a variation of the standard approach used in 3D printing and Computer Numerical Control (CNC) machining.

2.3.3 Accounting for Translation Error Between Core Samples

Difficulties arise when more than one core are added to the digitization queue. The ACRO has a theoretical 4.5 micron translational accuracy, but has not been achieved despite significant effort. These inaccuracies can cause drift in the images with relation to the core and result in the width of the core not being within the field of view of the images. We thus implemented a centering procedure that realigns the center of the core to the center of the image frame when the machine moves to a new sample.

First, the camera is moved to the (X_0, Y_0, Z_0) (Table S1) of the new core. From there, the camera is moved across a window, at constant velocity. The width of the window, w , in millimeters is defined in the machine configuration file and is editable. $(X_0 - 1/2 * w, Y_0, Z_0)$ to $(X_0 + 1/2 * w, Y_0, Z_0)$. Images are captured at equal distance intervals analogously to the image focusing procedure. Once again, the image with the highest normalized variance score is considered the best image and its location is used as the realigned X_0 . This procedure drastically improves digitization quality of batches of cores.

2.3.4 Stitching

Image stitching is a well explored field, ranging from panoramic images taken on smart phones to highly tuned microscopy slide stitching. Stitching one image to another requires both to share a region of overlap. When capturing a sample using TIM, the operator has the ability to choose a percentage amount of overlap between images. Most samples are digitized with a percentage overlap between 33% and 50%.

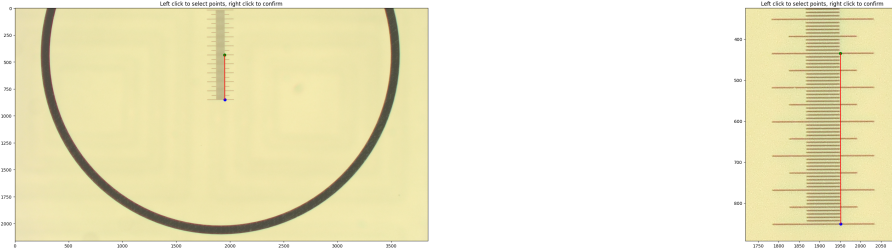
After testing numerous image stitching software APIs, we found the Python package Stitch2D most capable of stitching our images successfully. This package wraps OpenCV functions for finding distinctive image features using the SIFT feature detector and matches these features within the overlapping region of adjacent images (Lowe, 2004). The default implementation of the package produces high quality stitches but is memory inefficient. We implemented a few key memory conscious changes to the package and were able to run it on the Jetson without a problem.

Some tree ring analyses may not need the maximum scanning resolution produced by TIM. At maximum resolution, TIM's scans quickly produce large file sizes and can be costly to store at scale. To address this, a parameter in the machine configuration file allows the operator to choose a downsizing ratio to apply to images before they are stitched, decreasing the file size of the scans. With the same images, multiple final stitched resolutions can be made.

3 Results & Discussion

TIM is capable of producing extremely high resolution scans. We calculated the maximum dots per inch (DPI) at 21 140 of individual images captured from the system using a microscopy slide scale (with 0.01 mm graduations, Figure 4), and developed a Python tool to replicate this for varied lens focal lengths. When downscaling the final stitch, DPI scales linearly with the downscale percentage defined in the machine parameters.

Digitizing samples takes significantly longer for cookies than it does for cores (Figure 5). This is due to the surface area of cookies requiring more images as it has a square relationship to sample radius. For large cookies, the operator can choose to selectively



(a) Scale Bar for DPI measurements

(b) Zoomed in Scale Bar

Figure 4: Example of a single DPI measurement using a 0.01 mm slide scale. We found the DPI measured at multiple locations in the field of view vertically and horizontally converged on the same value.

scan a radius of the cookie instead of the whole surface. A single radius contains a portion of each ring. Scanning complete cookies at maximum DPI is unrealistic as file size limits are quickly encountered with small diameter cookies. To fit into the maximum 2.5 GB limits of a TIFF file, the maximum diameter of a cookie scanned at 30% of maximum resolution is limited to approximately 130 mm. This maximum cookie diameter is significantly smaller than the maximum core sample length. At maximum resolution, the file size limit constrains core samples to approximately 1 500 mm in length (though a larger ACRO frame than shown here would be needed to support this sample length). Samples larger than this limit can still be scanned, but TIM saves them as an uncompressed binary NumPy memory-mapped array file is produced. Currently, NumPy files are not supported by standard image viewers like ImageJ and would require custom tools to work with.

3.1 Strengths and Opportunities

TIM’s design minimizes the barriers to build an affordable, efficient and high-resolution image capture system in smaller labs without compromising scan quality, and while allowing scanning of cookies and cores. We have measured tree ring widths using the digitized samples from TIM using CooRecorder as well as ImageJ. Publicly available tree-ring datasets can be found on multiple online repositories such as TreeSource’s Tree-Rings Database for Canadian sites or the International Tree-Ring Data Bank (ITRDB) for worldwide data (Girardin *et al.*, 2021) (Grissino-Mayer & Fritts, 1997). Both of these databases offer metadata rich data on measured tree-rings but do not store the source images of samples. One opportunity for this development could come as more universal and large-scale open-data storage of tree ring images come online. Such open repositories would also increase the value of developing new frameworks count vessel or identify rings, which are already starting and have the potential to greatly decrease the time invested in manually identifying tree anatomy (Resente *et al.*, 2021) (Poláček *et al.*, 2023). With these more fully developed TIM could be extended to be run such frameworks while scanning, possibly taking additional scans only when needed to reach sufficient algorithm accuracy.

We tested a scanned cookie of size (HEIGHT)X(WIDTH) (WAITING FOR SANDY) pixels from TIM with the R-CNN presented by Poláček *et al.* on two servers. The first being the high-performance UBC ARC Sockeye which completed the task in 15 minutes.

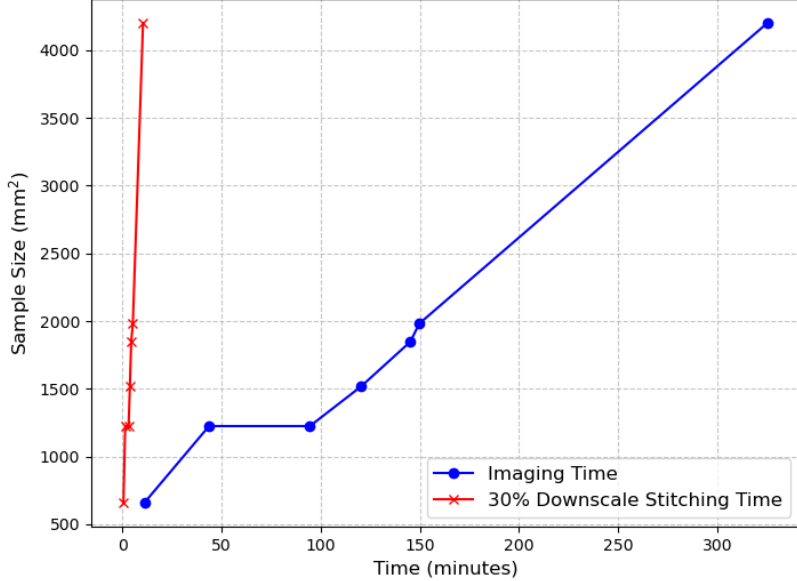


Figure 5: Time to digitize a sample is dependent on the sample’s surface area and the desired final resolution. Cores benefit from linear surface area to sample length. The range of sample included are from a 3mm x 220mm core to a 75mm x 56mm cookie. True sampling times are drastically influenced by configurable machine parameters.

As many do not have access to such powerful computing, we also tested the same image on an RTX A6000 GPU server—taking 3.5 hours to complete the task for approximately \$3.50 USD. While the results of automated tree rings are promising, further testing is necessary to test the feasibility of running this model on an edge computer or developing integrations for TIM with a remote server.

Finally, an exciting frontier for machines such as TIM is integrating additional sensors. While much of the current imaging time of samples comes from taking a vertical stack of images to obtain one in-focus image, advanced microscopy applications have overcome similar challenges through supplemental sensors that measure the distance between the subject and lens. Adding such sensor support and a control loop to focus images could significantly reduce sampling time on the scale of an order of magnitude. Using rotary encoders on each of the motors controlling the X and Y movement would be a welcomed addition—this would greatly increase the accuracy of the the location of the camera on the work plane.

4 Conclusion

By taking advantage of a common three degree of freedom cartesian machine design, powerful edge computing, and a microscope camera we were able to design a cost effective and high resolution digitization tool for wood samples. We significantly increased the maximum sample length and maximum resolution compared to common alternatives in the field. In addition, the machine design was intended to be readily replicated by labs with minimal engineering experience and equipment.

4.1 Supplemental Information

Table S1: Mathematical notation used in this paper.

Terms	Math Notation
X_0, Y_0, Z_0	The initial cartesian coordinates of the camera when the sample is saved by the user.
(X_k, Y_k, Z_k)	A unique set of X , Y , and Z coordinates for the center point of an individual image k .
(X_{k+1}, Y_{k+1})	The X and Y coordinates of an image that neighbors image k at (X_k, Y_k) .
δ	Equally spaced heights, relative to Z_0 , to capture images at and use to find a sharp image.
α_k	The response variable of the PID control algorithm which adjusts the initial height of an image to gradually align $Z_{focused}$ to be at the center index of $\mathbf{Z}_{samples}$.
$NV()$	Normalized variance 'function.'
$Z_{focused}$	The Z value of the most in-focus image in $\mathbf{Z}_{samples}$.
$\mathbf{Z}_{samples}$	A vector containing the Z coordinate for multiple images at the same X_k, Y_k .
$i_{\max, k}$	The index of the image with the largest normalized variance at the same (X_k, Y_k) .
	$i_{\max} = \arg \max_i NV(image(\mathbf{Z}_{samples}))$
w	The width of the window to traverse when trying to center a core.
$image()$	The image at a corresponding Z value from $\mathbf{Z}_{samples}$.
d_1	The relative distance from the camera to one edge of a leveled sample.
d_2	The relative distance from the camera to the opposite edge of a leveled sample.

References

- Buechling, A., Martin, P.H. & Canham, C.D. (2017) Climate and competition effects on tree growth in Rocky Mountain forests. *Journal of Ecology* **105**, 1636–1647, eprint: <https://onlinelibrary.wiley.com/doi/pdf/10.1111/1365-2745.12782>.
- Canham, C.D., LePage, P.T. & Coates, K.D. (2004) A neighborhood analysis of canopy tree competition: effects of shading versus crowding. *Canadian Journal of Forest Research* **34**, 778–787, publisher: NRC Research Press.
- Fritts, H.C. (1971) Dendroclimatology and dendroecology. *Quaternary Research* **1**, 419–449.
- García-Hidalgo, M., García-Pedrero, A., Colón, D., Sangüesa-Barreda, G., García-Cervigón, A.I., López-Molina, J., Hernández-Alonso, H., Rozas, V., Olano, J.M. & Alonso-Gómez, V. (2022) CaptuRING: A do-it-yourself tool for wood sample digitization. *Methods in Ecology and Evolution* **13**, 1185–1191, eprint: <https://onlinelibrary.wiley.com/doi/pdf/10.1111/2041-210X.13847>.
- Girardin, M.P., Guo, X.J., Metsaranta, J., Gervais, D., Campbell, E., Arsenault, A., Isaac-Renton, M., Harvey, J.E., Bhatti, J. & Hogg, E.H. (2021) A national tree-ring data repository for Canadian forests (CFS-TRenD): structure, synthesis, and applications. *Environmental Reviews* **29**, 225–241, publisher: NRC Research Press.
- Griffin, D., Porter, S.T., Trumper, M.L., Carlson, K.E., Crawford, D.J., Schwalen, D. & McFadden, C.H. (2021) Gigapixel Macro Photography of Tree Rings. *Tree-Ring Research* **77**, 86–94, publisher: Tree-Ring Society.
- Grissino-Mayer, H.D. & Fritts, H.C. (1997) The International Tree-Ring Data Bank: an enhanced global database serving the global scientific community. *The Holocene* **7**, 235–238, publisher: SAGE Publications Ltd.
- Guay, R., Gagnon, R. & Morin, H. (1992) A new automatic and interactive tree ring measurement system based on a line scan camera. *The Forestry Chronicle* **68**, 138–141.
- Guibal, F. & Guiot, J. (2021) Dendrochronology. *Paleoclimatology* (eds. G. Ramstein, A. Landais, N. Bouttes, P. Sepulchre & A. Govin), pp. 117–122, Springer International Publishing, Cham.
- Levanič, T. (2007) Atrics – A New System for Image Acquisition in Dendrochronology. *Tree-Ring Research* **63**, 117–122, publisher: Tree-Ring Society.
- Lowe, D.G. (2004) Distinctive Image Features from Scale-Invariant Keypoints. *International Journal of Computer Vision* **60**, 91–110.
- Mann, M.E., Bradley, R.S. & Hughes, M.K. (1999) Northern hemisphere temperatures during the past millennium: Inferences, uncertainties, and limitations. *Geophysical Research Letters* **26**, 759–762, eprint: <https://onlinelibrary.wiley.com/doi/pdf/10.1029/1999GL900070>.
- McMillin, C.W. (1982) Application of Automatic Image Analysis to WoodScience. *Wood Science* **14**, 97–105.

- Mir, H., Xu, P. & Van Beek, P. (2014) An extensive empirical evaluation of focus measures for digital photography. p. 90230I, San Francisco, California, USA.
- Mohammadi, F.S., Shabani, H. & Zarei, M. (2024) Fast and robust feature-based stitching algorithm for microscopic images. *Scientific Reports* **14**, 13304, publisher: Nature Publishing Group.
- Muhlich, J.L., Chen, Y.A., Yapp, C., Russell, D., Santagata, S. & Sorger, P.K. (2022) Stitching and registering highly multiplexed whole-slide images of tissues and tumors using ASHLAR. *Bioinformatics (Oxford, England)* **38**, 4613–4621.
- O'Dwyer, A. (2000) A Summary of PI and PID Controller Tuning Rules for Processes with Time Delay. Part 1: PI Controller Tuning Rules. *IFAC Proceedings Volumes* **33**, 159–164.
- Poláček, M., Arizpe, A., Hüther, P., Weidlich, L., Steindl, S. & Swarts, K. (2023) Automation of tree-ring detection and measurements using deep learning. *Methods in Ecology and Evolution* **14**, 2233–2242, eprint: <https://onlinelibrary.wiley.com/doi/pdf/10.1111/2041-210X.14183>.
- Propst, S. & Mueller, J. (2025) Time Code for multifunctional 3D printhead controls. *Nature Communications* **16**, 1035, publisher: Nature Publishing Group.
- Resente, G., Gillert, A., Trouillier, M., Anadon-Rosell, A., Peters, R.L., von Arx, G., von Lukas, U. & Wilmking, M. (2021) Mask, Train, Repeat! Artificial Intelligence for Quantitative Wood Anatomy. *Frontiers in Plant Science* **12**, publisher: Frontiers.
- Ro, S.H. & Kim, S.H. (2021) An image stitching algorithm for the mineralogical analysis. *Minerals Engineering* **169**, 106968.
- Robinson, W.J. & Evans, R. (1980) A MICROCOMPUTER -BASED TREE -RING MEASURING SYSTEM. *Tree-Ring Bulletin* **40**.
- Sheppard, P.R. (2010) Dendroclimatology: extracting climate from trees. *WIREs Climate Change* **1**, 343–352, eprint: <https://onlinelibrary.wiley.com/doi/pdf/10.1002/wcc.42>.
- Speer, J.H. (2010) *Fundamentals of Tree Ring Research*. University of Arizona Press.
- Williams, A.P., Michaelsen, J., Leavitt, S.W. & Still, C.J. (2010) Using Tree Rings to Predict the Response of Tree Growth to Climate Change in the Continental United States during the Twenty-First Century Section: Earth Interactions.